AC conductivity of nanoporous metal-oxide photoanodes for solar energy conversion

Steven J. Konezny, Diyar Talbayev, Ismail El Baggari, Charles A. Schmuttenmaer, and Victor S. Batista

Department of Chemistry, Yale University, P.O. Box 208107, New Haven, CT 06520-8107

ABSTRACT

The temperature- and frequency-dependent ac conductivity of nanoporous metal-oxide semiconductors commonly used in technologies for solar photoconversion is analyzed using a model based on fluctuation-induced tunneling conduction (FITC). The model takes into account the potential barriers at the regions of nanoparticle contact that limit electron transport. In contrast to previous models, quantitative agreement is found with the FITC model with a single set of parameters over the entire temperature range studied. Guidelines for the design of new materials for dye-sensitized solar cells (DSSCs) and solar photocatalysis are discussed.

Keywords: charge transport, nanoporous metal oxides, tunneling, AC conductivity, solar cells, photocatalytic cells

1. INTRODUCTION

The discovery of low-cost high-efficiency dye-sensitized solar cells (DSSCs) (i.e., exceeding 10% solar-to-electric energy conversion efficiency) exploited the large surface area of nanoporous thin films made by sintering TiO_2 nanoparticles (≈ 50 m^2/g).[1–3] When sensitized with dye molecules, these nanoporous films yield photoanodes with large optical density and therefore high light-harvesting efficiency.[4,5] Methods to enhance electron injection into the TiO_2 conduction band have been found, including filling the nanopores with electrolyte solutions containing two-electron redox couples (e.g., I^-/I^{3-}) that efficiently regenerate the photooxidized dye adsorbates and transport holes to the cathode. In addition, Lewis-base adsorbates such as terbutyl pyridinum have been found to passivate the exposed (non-sensitized) TiO_2 surface, suppressing recombination of the photoinjected electron with redox species in solution. However, charge recombination and trapping are still thought to be efficiency-limiting factors since the conductivity of TiO_2 films is rather low ($\sigma_{dc} \approx 10^{-13}$ $\Omega^{-1}cm^{-1}$),[6] much lower than the conductivity of TiO_2 single crystals ($\sigma_{dc} \approx 10$ $\Omega^{-1}cm^{-1}$),[7,8] and thus the transport time of an electron percolating through a typical few-micron TiO_2 film is significant ($\approx 1 - 10$ ms).[9,10] Therefore, the outstanding challenge is to understand the phenomena that limit electron transport18 and obtain guidelines for optimizing the conductivity of nanoporous thin films without increasing the recombination rate. To ensure efficient charge carrier collection, the electron transport time through the TiO_2 film should be significantly shorter than the average recombination time.

Despite nearly two decades of intense research in DSSCs, there is no generally accepted model to describe charge transport in nanoporous TiO_2. Trapping/detrapping mechanisms similar to those commonly used for amorphous silicon19 were initially found to be in agreement with transient measurements of photogenerated electrons in DSSCs.[11,12] However, more recent studies have raised concerns due to the significant discrepancy in the distribution of traps determined by different experimental techniques[13,14] and the much weaker temperature dependence of the diffusion coefficient than expected.[13,15] In addition, the models that involve multiple-trap-and-release (MTR) of charge carriers in an exponential distribution of traps or variable-range hopping (VRH) between defects both predict a temperature dependence of the form $\ln\sigma \propto T^{-\alpha}$, with $\alpha = 1/4$ for MTR[16] and $\alpha = 1/4$ for VRH.[17] These models are therefore have a limite range of validity since they are unable to account for the saturation of σ_{dc} at low temperatures observed in this work (Fig. 1) and elsewhere[6,18–21] without

Further author information: (Send correspondence to S.J.K. or V.S.B.)
S.J.K.: E-mail: steven.konezny@yale.edu, Telephone: 1 203 432 5911
V.S.B.: E-mail: victor.batista@yale.edu, Telephone: 1 203 432 6672

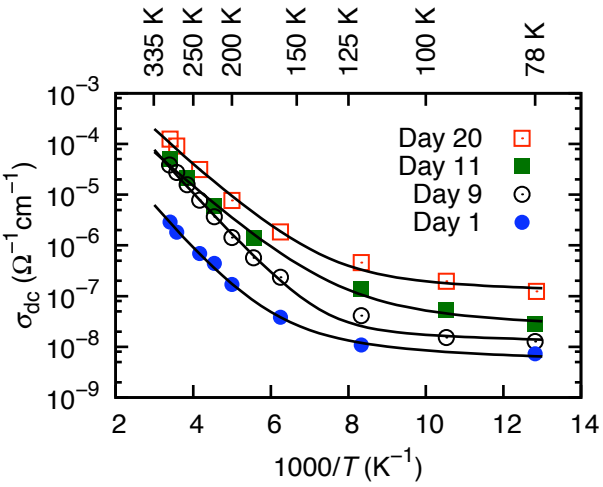

Figure 1. Temperature dependence of the DC conductivity of the SnO_2 sample. Solid lines illustrate the FITC model fitting. The corresponding fitting parameters are listed in Table 1.

relying on multiple parallel mechanisms. These data are consistent with recent transient absorption spectroscopy studies of bare and dye-sensitized nanocrystalline TiO_2 films show that the recombination rate follows the same temperature dependence as σ_{dc}.[22]

We recently reported dark DC conductivity measurements of nanoporous TiO_2 films over a wide temperature range ($T = 78 - 335$ K) and demonstrated a good agreement with the FITC model,[6] in which the transport is determined by tunnelling conduction through contact junctions connecting sintered nanoparticles. The FITC model predicts temperature-independent conductivity reflecting simple inelastic tunnelling at low temperature that makes a gradual transition to thermally activated behaviour at high temperature. For typical TiO_2 thin-film dimensions and preparation conditions, the asymptotic low-temperature conductivity is small ($\sigma_{dc} \approx 10^{-13}$ Ω^{-1}cm^{-1}) and therefore difficult to measure. In fact, most conductivity measurements reported to date have been limited to the high-temperature regime where the Arrhenius prediction of the FITC model is indistinguishable from models solely based on thermally activated processes. It is therefore not surprising that the FITC mechanism has been largely overlooked. In this article, we show that the FITC theory can be extended to quantitatively describe dark AC conductivity measurements in nanoporous SnO_2 films. These results suggest that the FITC mechanism is responsible for electron transport in a wide variety of nanoporous metal-oxide materials that share the same electrically inhomogeneous microstructure.

2. CONDUCTIVITY IN NANOPOROUS METAL OXIDES

2.1 Power-Law Dependence of the AC Conductivity

The total measured AC conductivity can often be separated into frequency-dependent and DC components and expressed as

$$\sigma(\omega) = \sigma_{dc} + \sigma'(\omega), \tag{1}$$

where $\sigma'(\omega)$ is the frequency-dependent component of the total conductivity σ. In a wide variety of disordered materials, including the systems studied in this work, $\sigma'(\omega)$ has a power-law form,[?,23,24]

$$\sigma'(\omega) = c\omega^s, \tag{2}$$

where both the power-law coefficient c and exponent s have temperature and frequency dependences that are indicative of the underlying charge transport mechanism. The functional form of these parameters have been derived for many different models based on quantum mechanical tunneling or hopping cases. For example, the VRH model predicts a temperature-independent though frequency-dependent s with a value of 0.8 for a typical characteristic relaxation time of 10^{-13} s^{-1} and a frequency of 10 kHz.[24] The correlated barrier hopping model also has a frequency-dependent s, though its value tends toward $s = 1$ as $T \to 0$ K.[?]

2.2 Low Frequency / DC Conductivity

Building upon FITC models previously applied to describe conductivity in other systems of comparable microstructure,[6,25–27] we model the TiO_2 thin films as networks of contact junctions where noncrystalline TiO_2 regions connect the crystalline anatase centers of TiO_2 nanoparticles (see the SEM images in **??** and the representations depicted in **??**). The tunneling rate across a junction depends on the effective area A at the region of closest approach between crystallites, the effective tunneling width w of the noncrystalline region of the junction, and the zero-field barrier height φ_0, which is primarily the result of the conduction-band offset between the crystalline and noncrystalline TiO_2 phases.

With typical junction parameters (e.g., $A \approx 50$ nm^2, $w \approx 3-4$ nm; see Table 1) and a static dielectric constant of $\varepsilon_r \approx 20$ inside the junction, the effective junction capacitance $C = \varepsilon_r \varepsilon_0 A/w$ is very small (on the order of 10^{-6} pF). Therefore, thermal fluctuations in the density of the free electrons near the junction generate strong voltage fluctuations V_T with $\langle V_T^2 \rangle = k_B T/C$, where k_B is the Boltzmann constant. Upon averaging, these fluctuations can increase the tunneling probability by effectively reducing the width and height of the barrier due to the superposition of the applied and thermally generated electric fields. Note that the resulting Boltzmann distribution $P(\mathcal{E}) = (a/\pi k_B T)^{1/2} exp(\mathcal{E}^2/k_B T)$ of thermally generated electric field fluctuations $\mathcal{E}_T = V_T/w$, has a width related to the charging energy $E_c = CV_T^2/2 = a\mathcal{E}_T^2$ required to displace the capacitor from equilibrium, where $a = \varepsilon_r \varepsilon_0 A w/2$.

The resulting fluctuation-induced tunneling conductivity of the TiO_2 thin film is

$$\sigma_{dc}(\mathcal{E}) = \frac{\gamma \langle j_{dc}(\mathcal{E}) \rangle A}{t V}, \tag{3}$$

where t is the thickness of the sample, V is the voltage across the junction, γ is the sheet-conductance proportionality constant,[28] and $\langle j(\mathcal{E}) \rangle$ is the thermal average of the net current density $j(\mathcal{E})$ in the direction of the applied field:[6,27]

$$\begin{aligned} j_{dc}(\mathcal{E}) = \frac{mqk_B^2 T^2}{2\pi^2 \hbar^3} \Bigg(& \left\{ \frac{e^{-2\chi w\xi}}{T'^2} \left(1 - e^{-T' q\mathcal{E}w/k_B T}\right) \right\} + \left\{ \frac{e^{-2\chi w\xi}}{1+T'} \left(1 - e^{-T' q\mathcal{E}w/k_B T}\right) \right\} \\ & + \left\{ e^{-\varphi_m/k_B T} \left(1 - e^{-q\mathcal{E}w/k_B T}\right) \right\} + \left\{ \frac{e^{-2\chi w\xi}}{1-T'} \left[\left(1 - e^{-(1-T')\varphi_m/k_B T}\right) \right.\right. \\ & \left.\left. - \left(1 - e^{-(1-T')(\varphi_m + q\mathcal{E}w)/k_B T}\right) e^{-T' q\mathcal{E}w/k_B T} \right] \right\} \Bigg), \end{aligned} \tag{4}$$

where $\hbar$ is the reduced Planck constant, m is the charge carrier mass, q is the electron charge, $\chi = \left(2m\varphi_0/\hbar^2\right)^{1/2}$ is the tunneling constant, the dimensionless temperature-dependent parameter is given by $T' = 2\chi w \eta k_B T/\varphi_0$, and φ_m is the maximum in the field-corrected barrier. The dimensionless parameters ξ and η are field dependent and originate from the first two terms in a power series expansion of the exponent of the transmission coefficient under the WKB approximation.[29] The conductivity as expressed in Eqs. 3 and 4 is more explicit than the low-field, low-temperature approximation $\sigma \approx \sigma_0 \exp\left[-T_1/(T_0+T)\right]$ frequently used in the literature, where σ_0, T_0 and T_1 are temperature-independent parameters. This simplified expression has a limited range of validity and does not give accurate junction parameter values.

Both the Arrhenius and temperature-independent regimes in the observed fluctuation-induced tunneling conductivity are described by 4. Each of the four terms in curly brackets includes a forward current density component in the direction of the applied electric field and a backflow current density in the opposite direction. The first term is the net current density in the low-temperature limit, with an abrupt change in the density of states at the Fermi energy, while the other terms are corrections obtained by expanding the Fermi-Dirac distribution to first order in temperature. The second term corresponds to the correction to the density of occupied states below the Fermi energy. The third term is the net current density due to electrons in the exponential tail of the distribution above the Fermi energy that are higher in energy than φ_m and are assumed to have a transmission coefficient equal to one (i.e., thermal activation over the barrier). The last term in curly brackets is the net current density of electrons at energies above the Fermi energy with a transmission coefficient less than one (i.e., thermally activated tunneling).

3. EXPERIMENTAL METHODS

We performed AC impedance and DC resistance measurements on sintered SnO_2 nanoparticle films. Nanoparticles with diameter of 22-43 nm where purchased from Alfa Aesar (Tin (IV) oxide, NanoArc). Nanoparticle sludge was prepared from 1.1 g of nanoparticle powder and 1 ml of distilled water by mixing with pestle and mortar and subsequently was spread onto a bottom electrode between two fiberglass spacers, which are 200 $\pm$ 4 μm thick with measured resistance $>$ 200 TΩ. Immediately thereafter, the top electrode was applied, and the sandwich was clamped together with screws. The sample was dried for 1 week at room temperature and then annealed in air at 450 °C for 40 minutes, the typical sintering conditions used for SnO_2 in DSSCs.**??** The sample electrodes were high chromium content stainless steel (grade 309). For temperature-dependent DC and AC resistance measurements, the SnO_2 sample was loaded (after being kept for 20 days at room temperature) in a cryostat (Janis ST-100) and kept in the dark under vacuum ($<$ 10 mTorr). A Stanford Research Systems SR570 low-noise current preamplifier was used to measure the current that passes through the sample in a two-terminal measurement. The applied bias voltage was 0.2 V, and the sample displayed a linear I-V curve at room temperature at bias voltages up to 1 V. AC impedance was measured in the 0.3 - 30000 Hz range using a Stanford Research Systems SR830 digital lockin amplifier using the AC bias of 0.25 and 1 V.

4. RESULTS AND DISCUSSION

Figure 2(a) shows the frequency dependent conductivity as a function of temperature recorded on day 1 of measurements. The conductivity clearly displays a low-frequency region where it is equal to the measured DC conductivity and is independent of frequency. At low tempetrature and high frequencies, the power law dependence is also clearly observed. The solid lines in Fig. 2 illustrate a least-squares fit using the power law of equations (1) and (2). Figure 3 shows the temperature dependence of parameter c extracted from the least-squares fit for several measurement days. The parameter s was kept constant in the fits, as the rather narrow frequency window for the power law dependence prevented us from a detailed study of its temperature dependence. Such study of the power law parameter behavior will be the subject of a separate publication. In this article, we discuss the temperature behavior of the DC conductivity in SnO_2 films and show that it is well described by the FITC model.

Table 1. Nanocrystallite diameter $d_{\rm nc}$ measured by XRD and FITC model fitting parameters used for samples A and B in Fig. **??**. A, w, and φ_0 are the effective area, width, and zero-field barrier height of the junction, respectively, and d_j is the effective junction diameter given by $d_j \equiv 2\sqrt{A/\pi}$.

		s	φ_0 (meV)	w (nm)	A (nm^2)	d_j (nm)
Sintered SnO_2 nanoparticle film	Day 1	1.23	166	3.13	5.58	2.67
Sintered SnO_2 nanoparticle film	Day 9	1.13	137	3.68	44.2	7.50
Sintered SnO_2 nanoparticle film	Day 11	1.09	113	3.49	11.6	3.83
Sintered SnO_2 nanoparticle film	Day 20	DC only	102	3.43	29.7	6.14

Figure 1 shows the temperature dependence of the DC conductivity on several measurement days spanning a 20-day period. Figs. 2(a)-(c) also show the evolution of the frequency dependent conductivity between days 1 and 11 of measurements. The conductivity of the sample steadily grows with time and saturates after 20-25 days (Fig. 2(d)). Such aging of the sintered SnO_2 film is hardly surprising, as it is well known that the nanoporous semiconductor films are highly sensitive to the environment due to their large surface areas, a fact famously exploited in sensor applications.[30,31] We ascribe the aging to a slow adsorption of contaminants on the surface of our nanoporous SnO_2 sample, even though at present we cannot pinpoint which contaminant dominates the conductivity drift. As we show in the following paragraphs, the effect of contaminant adsorption is well understood in the framework of FITC.

The application of the FITC model to DC transport in nanoporous TiO_2 was desribed in detail in our previous work.[6] We treat the nanoporous film as a resistor network where each resistor represents a tunneling junction

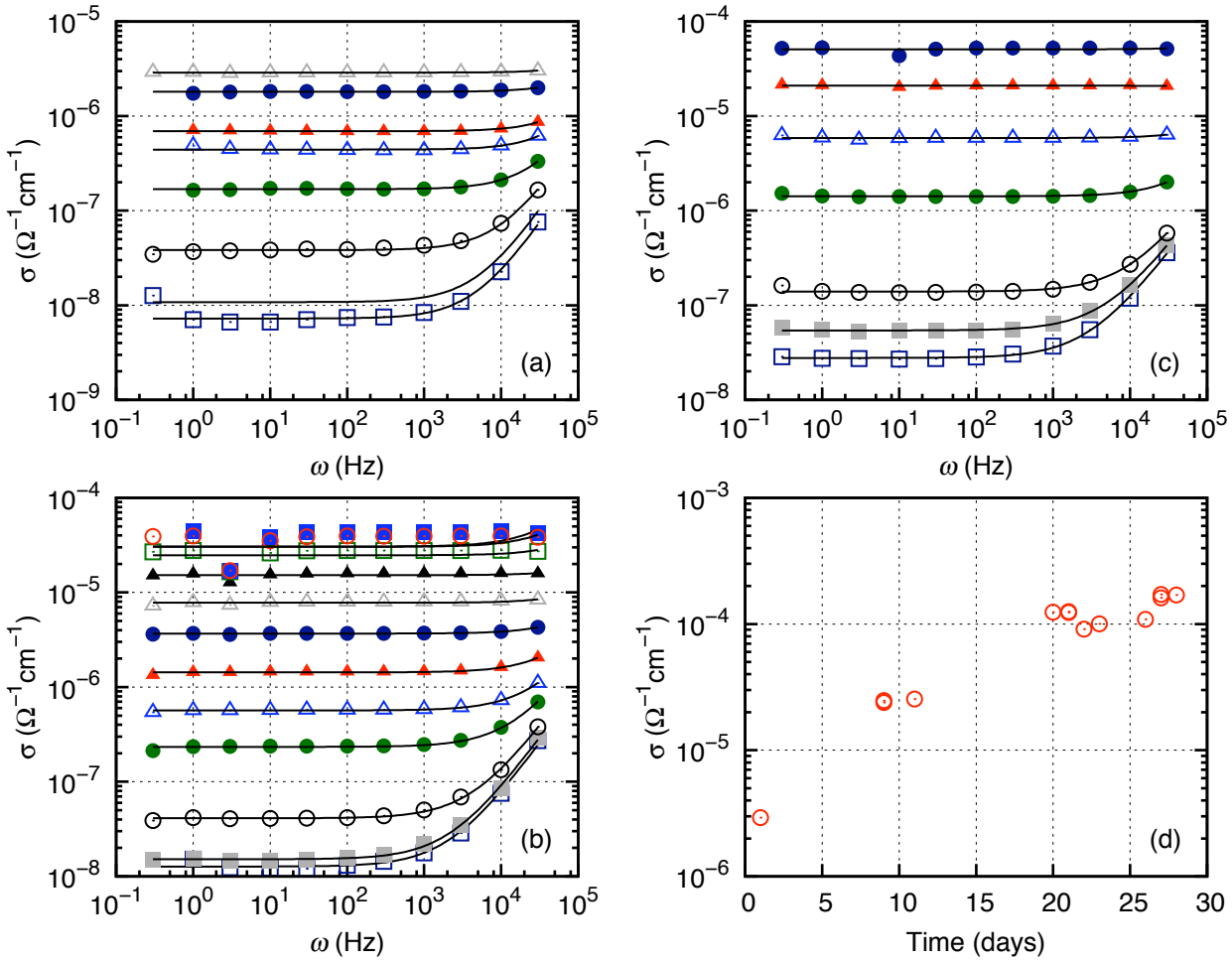

Figure 2. (a), (b), and (c): Frequency-dependent AC conductivity of the SnO_2 sample as a function of temperature measured on days 1, 9, and 11. Solid lines illustrate power law fits to equations (1) and (2). (d): Drift of the DC conductivity over the course of 28 days of measurement.

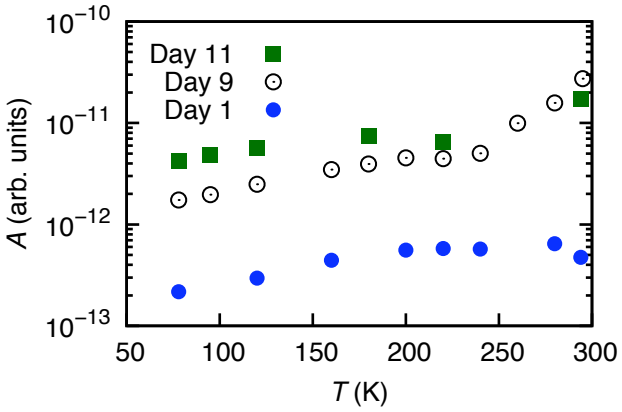

Figure 3. Temperature dependence of the power law parameter c, equation (2).

between sintered nanoparticles. The tunneling junction is created during sintering, when the amorphous shells of the crystalline nanoparticles fuse together to form a necking region.[6] The nanoparticle network is modeled by a triangular network of resistors, and a series of equivalent circuit transformations is carried out numerically until the whole network is replaced by single resistor with proportional to that of a single tunneling junction between nanoparticles. The temperature dependence of the single junction resistance is in turn described by the FITC model. We find that the measured conductivity is well described by the model at all stages of sample aging. The results of FITC model fitting are shown by solid lines in Fig. 1, and the fitting parameters are listed in Table 1. The parameters include the potential barrier height at the junction φ_0, the junction width w, and the area A and the diameter d_j of the junction connected by $A = \pi d_j^2/4$. We find that the junction width w does not change as the sample ages, which speaks against a slow "flow" or physical rearrangement of the nanoparticles. We observe no systematic change in junction diameter d_j. The large spread in the obtained values of d_j results from a low sensitivity of the FITC fitting procedure to parameters d_j and A compared to w and φ_0: the tunneling current is merely proportional to A, while it depends exponentially on w and φ_0. This also highlights the main observation of Table1 - a systematic lowering of the tunneling barrier φ_0 as the sample ages. This is consistent with the continuing contaminant adsorption on the surface of SnO_2 nanoparticles during aging. The adsorption can result in midgap electronic states in the necking region that effectively lower the tunneling barrier.

Our DC resistance measurements on sintered SnO_2 nanoparticle films show that the FITC description of electronic transport may have a broad applicability for mesoporous oxide semiconductor DSSC electrodes. ...

ACKNOWLEDGMENTS

The authors acknowledge support from the Chemical Sciences, Geosciences, and Biosciences Division, Office of Basic Energy Sciences, Office of Science, U.S. DOE (grant DE-FG02-07ER15909) and the NSF (Graduate Research Fellowship to ARP and grants ECCS-0404191 and CHE 0911520 for preliminary work).

REFERENCES

[1] B. O'Regan and M. Grätzel, "A low-cost, high-efficiency solar-cell based on dye-sensitized colloidal tio$_2$ films," *Nature* **353**(6346), pp. 737–740, 1991.

[2] M. K. Nazeeruddin, A. Kay, I. Rodicio, R. Humphrybaker, E. Mller, P. Liska, N. Vlachopoulos, and M. Grätzel, "Conversion of light to electricity by cis-x2bis(2,2-bipyridyl-4,4-dicarboxylate)ruthenium(ii) charge-transfer sensitizers (x = cl-, br-, i-, cn-, and scn-) on nanocrystalline tio$_2$ electrodes," *J. Am. Chem. Soc.* **115**(14), pp. 6382–6390, 1993.

[3] C.-Y. Chen, M. Wang, J.-Y. Li, N. Pootrakulchote, L. Alibabaei, C.-h. Ngoc-le, J.-D. Decoppet, J.-H. Tsai, C. Grtzel, C.-G. Wu, S. M. Zakeeruddin, and M. Grätzel, "Highly efficient light-harvesting ruthenium sensitizer for thin-film dye-sensitized solar cells," *ACS Nano* **3**(10), pp. 3103–3109, 2009.

[4] C. J. Barbe, F. Arendse, P. Comte, M. Jirousek, F. Lenzmann, V. Shklover, and M. Grätzel, "Nanocrystalline titanium oxide electrodes for photovoltaic applications," *J. Am. Ceram. Soc.* **80**(12), pp. 3157–3171, 1997.

[5] M. Grätzel, "Mesoscopic solar cells for electricity and hydrogen production from sunlight," *Chem. Lett.* **34**(1), pp. 8–13, 2005.

[6] S. J. Konezny, C. Richter, R. C. Snoeberger III, A. R. Parent, G. W. Brudvig, C. A. Schmuttenmaer, and V. S. Batista, "Fluctuation-induced tunneling conductivity in nanoporous TiO_2 thin films," *J. Phys. Chem. Lett.* **2**(0), pp. 1931–1936, 2011.

[7] L. Forro, O. Chauvet, D. Emin, L. Zuppiroli, H. Berger, and F. Levy, "High-mobility n-type charge-carriers in large single-crystals of anatase (tio_2)," *J. Appl. Phys.* **75**(1), pp. 633–635, 1994.

[8] H. Tang, K. Prasad, R. Sanjines, P. E. Schmid, and F. Levy, "Electrical and optical properties of tio_2 anatase thin-films," *J. Appl. Phys.* **75**(4), pp. 2042–2047, 1994.

[9] P. M. Sommeling, B. C. O'Regan, R. R. Haswell, H. J. P. Smit, N. J. Bakker, J. J. T. Smits, J. M. Kroon, and J. A. M. van Roosmalen, "Influence of a $ticl_4$ post-treatment on nanocrystalline tio_2films in dye-sensitized solar cells," *J. Phys. Chem. B* **110**(39), pp. 19191–19197, 2006.

[10] B. van der Zanden and A. Goossens, "The nature of electron migration in dye-sensitized nanostructured tio_2," *J. Phys. Chem. B* **104**(30), pp. 7171–7178, 2000.

[11] P. E. de Jongh and D. Vanmaekelbergh, "Trap-limited electronic transport in assemblies of nanometer-size tio_2 particles," *Phys. Rev. Lett.* **77**(16), pp. 3427–3430, 1996.

[12] J. Nelson, "Continuous-time random-walk model of electron transport in nanocrystalline tio_2 electrodes," *Phys. Rev. B* **59**(23), pp. 15374–15380, 1999.

[13] G. Boschloo and A. Hagfeldt, "Activation energy of electron transport in dye-sensitized tio_2 solar cells," *J. Phys. Chem. B* **109**(24), pp. 12093–12098, 2005.

[14] J. R. Jennings, A. Ghicov, L. M. Peter, P. Schmuki, and A. B. Walker, "Dye-sensitized solar cells based on oriented tio_2 nanotube arrays: Transport, trapping, and transfer of electrons," *J. Am. Chem. Soc.* **130**(40), pp. 13364–13372, 2008.

[15] N. Kopidakis, K. D. Benkstein, J. van de Lagemaat, A. J. Frank, Q. Yuan, and E. A. Schiff, "Temperature dependence of the electron diffusion coefficient in electrolyte-filled tio_2 nanoparticle films: Evidence against multiple trapping in exponential conduction-band tails," *Phys. Rev. B* **73**(4), p. 045326, 2006.

[16] T. Tiedje, J. M. Cebulka, D. L. Morel, and B. Abeles, "Evidence for exponential band tails in amorphous silicon hydride," *Phys. Rev. Lett.* **46**(21), pp. 1425–1428, 1981.

[17] N. F. Mott and E. A. Davis, Oxford University Press, New York, 1971.

[18] A. K. Hassan, N. B. Chaure, A. K. Ray, A. V. Nabok, and S. Habesch, "Structural and electrical studies on sol-gel derived spun tio_2 thin films," *J. Phys. D-Appl. Phys.* **36**(9), pp. 1120–1125, 2003.

[19] E. Barborini, G. Bongiorno, A. Forleo, L. Francioso, P. Milani, I. Kholmanov, P. Piseri, P. Siciliano, A. Taurino, and S. Vinati, "Thermal annealing effect on nanostructured tio_2 microsensors by supersonic cluster beam deposition," *Sens. Actuators, B* **111-112**, pp. 22–27, 2005.

[20] K. Pomoni, A. Vomvas, and C. Trapalis, "Dark conductivity and transient photoconductivity of nanocrystalline undoped and n-doped tio_2 sol-gel thin films," *Thin Solid Films* **516**(6), pp. 1271–1278, 2008.

[21] K. M. Reddy, S. V. Manorama, and A. R. Reddy, "Bandgap studies on anatase titanium dioxide nanoparticles," *Mater. Chem. Phys.* **78**(1), pp. 239–245, 2003.

[22] R. Katoh and A. Furube, "Tunneling-type charge recombination in nanocrystalline TiO_2 films at low temperature," *J. Phys. Chem. Lett.* **2**(0), pp. 1888–1891, 2011.

[23] A. Jonscher, "The universal dielectric response," *Nature* , pp. 673–679, 1977.

[24] A. Long, "Frequency-dependent loss in amorphous semiconductors," *Adv. Phys.* **31**(5), pp. 553–637, 1982.

[25] P. Sheng, "Fluctuation-induced tunneling conduction in disordered materials," *Phys. Rev. B* **21**(6), pp. 2180–2195, 1980.

[26] S. Paschen, M. N. Bussac, L. Zuppiroli, E. Minder, and B. Hilti, "Tunnel-junctions in a polymer composite," *J. Appl. Phys.* **78**(5), pp. 3230–3237, 1995.

[27] S. J. Konezny, M. N. Bussac, and L. Zuppiroli, "Charge transport mechanisms in microcrystalline silicon," *Appl. Phys. Lett.* **92**(1), p. 012107, 2008.

[28] S. J. Konezny, M. N. Bussac, A. Geiser, and L. Zuppiroli, "Charge transport mechanisms in organic and microcrystalline silicon field-effect transistors," in *Organic Field-Effect Transistors VI*, Z. Bao and D. J. Gundlach, eds., *Proceedings of SPIE* **6658**, p. 66580D, SPIE, (Bellingham, WA), 2007.

[29] J. J. Sakurai, Addison-Wesley, Massachusetts, 1994.

[30] X. Chen and S. S. Mao, "Titanium dioxide nanomaterials: Synthesis, properties, modifications, and applications," *Chem. Rev.* **107**(7), pp. 2891–2959, 2007.

[31] M. Tiemann, "Porous metal oxides as gas sensors," *Chem. Eur. J.* **13**(30), pp. 8376–8388, 2007.